

Structure and magnetic properties of melilite-type compounds $\text{RE}_2\text{Be}_2\text{GeO}_7$ (RE = Pr, Nd, Gd-Yb) with Rare-Earth ions on Shastry-Sutherland lattice

Malik Ashtar,^{1□} Yuming Bai,^{1†} Longmeng Xu¹, Zongtang Wan¹, Zijun Wei¹, Yong Liu², Mohsin Ali Marwat³, Zhaoming Tian^{1*}

¹ Wuhan National High Magnetic Field centre and School of Physics, Huazhong University of Science and Technology, Wuhan 430074, Peoples R China.

² School of Physics, Wuhan University, Wuhan 430072, Peoples R China.

³ College of Materials Science and Engineering, Huazhong University of Science and Technology, Wuhan 430074, PR China

ABSTRACT:

Rare-earth (RE) based frustrated magnets as typical systems of combining strong spin-orbit coupling, geometric frustration and anisotropic exchange interactions, can give rise to diverse exotic magnetic ground states such as quantum spin liquid (QSL). The discovery of new RE-based frustrated materials is crucial for exploring the exotic magnetic phases. Herein, we report the synthesis, structure and magnetic properties of a family of melilite-type $\text{RE}_2\text{Be}_2\text{GeO}_7$ (RE = Pr, Nd, Gd-Yb) compounds crystallized in a tetragonal $P\bar{4}2_1m$ structure, where magnetic RE^{3+} ions lay out on Shastry-Sutherland lattice (SSL) within ab -plane and are well separated by nonmagnetic $[\text{GeBe}_2\text{O}_7]^{6-}$ polyhedrons along c -axis. Temperature (T)-dependent susceptibilities $\chi(T)$ and isothermal magnetization $M(H)$ measurements reveal that most $\text{RE}_2\text{Be}_2\text{GeO}_7$ compounds except RE=Tb show no magnetic ordering down to 2 K despite the dominant antiferromagnetic (AFM) interactions, where $\text{Tb}_2\text{Be}_2\text{GeO}_7$ undergoes AFM transition with Néel temperature $T_N \sim 2.5$ K and field-induced spin flop behaviors ($T < T_N$). In addition, the calculated magnetic entropy change ΔS_m from the isothermal $M(H)$ curves reveal a viable magnetocaloric effect (MCE) for $\text{RE}_2\text{Be}_2\text{GeO}_7$ (RE = Gd, Dy) in liquid helium temperature regimes, $\text{Gd}_2\text{Be}_2\text{GeO}_7$ shows maximum ΔS_m up to $54.8 \text{ J K}^{-1} \text{ Kg}^{-1}$ at $\Delta H = 7 \text{ T}$ and $\text{Dy}_2\text{Be}_2\text{GeO}_7$ has largest value $\Delta S_m = 16.1 \text{ J K}^{-1} \text{ kg}^{-1}$ at $\Delta H = 2 \text{ T}$ in this family. More excitingly, rich diversity of RE ions in this family enables an archetype for exploring exotic quantum magnetic phenomena with large variability of spin located on SSL lattice.

□ M Ashtar and YM Bai contribute equally to this work.* Corresponding author, email: tianzhaoming@hust.edu.cn

■ INTRODUCTION

Geometrically frustrated magnets as a fertile playground to explore the exotic quantum magnetic phases, have attracted enormous interest in condensed matter physics. In such systems, magnetic moments are located on the geometric lattices usually constructed by connections of corner or edge-shared triangular or tetrahedra lattices,¹⁻⁶ where geometric lattice network can be in two-dimension (2D) like triangular, kagome and honeycomb type, or in three-dimension like pyrochlore, garnet, and hyperkagome type. For 2D frustrated systems with spin $S=1/2$, competing confined spin exchange interactions restrict the magnetic degrees of freedom, lead to strong frustration accompanied by enhanced quantum fluctuations. Ultimately, the system is prevented from adopting conventional long-range magnetic ordering but in favour of non-trivial magnetic states like quantum spin liquid (QSL) state,^{2,7} typical examples include the 2D triangular lattice κ -(BEDT-TTF)₂Cu₂(CN)₃^{3,8} and 2D kagome lattice ZnCu₃(OH)₆Cl₂ and its derives,⁹⁻¹¹ which don't show long-range magnetic order or spin freezing with temperature down to milliKelvin temperatures as best candidate materials realizing QSL state. On the other hand, to unveil novel exotic magnetic states, extensive theoretical and experimental works have been dedicated to search for new frustrated materials on various lattices. A particular interesting structure in this respect is called Shastry-Sutherland lattice (SSL),¹² which consists of planes of orthogonal dimers with intradimer exchange J_1 and interdimer exchange J_2 as shown in Figure 1a. Since firstly proposed by Shastry and Sutherland as theoretical toy model,¹² it has received substantial attention to investigate novel quantum magnetic phenomena. In this SSL model, different magnetic ground states are predicted depending on the relative strength of J_1 and J_2 . When J_2/J_1 is large, it will support the Heisenberg antiferromagnetic (AFM) order, small J_2/J_1 will induce a disordered dimer singlet ground state, and insulating SrCu₂(BO₃)₂ exemplifies this disordered "spin liquid (SL)" regime.¹³⁻¹⁵ Moreover, intriguing quantum phase transition from AFM to SL phases can take place by tuning J_2/J_1 under the external magnetic field or high pressure.^{16,17} New material realizations on SSL motif will offer promising platform to study the predicted magnetic phases.

Quite recently, frustrated magnets incorporating $4f$ rare-earth (RE) ions attract intensive attention to explore exotic magnetic phases arising from the multiple interplay of spin-orbit entangled $j_{\text{eff}}=1/2$ moment, geometric lattice frustration, exchange dipolar interaction and diverse spin-types of RE³⁺.¹⁸⁻²² And indeed, a wide variety of exotic magnetic phases have been experimental identified, such as QSL,^{7,22} quantum spin ice^{18,23,24} and multipolar order,^{25,26} etc. In terms of the SSL systems, metallic RE₂Pt₂Pb (RE= Yb, Ce)^{27,28} and REB₄ (RE =Ce-Yb)^{29,30} compounds have been well studied, some of interesting magnetic phenomena have been reported, as examples, field-induced quantum phase transition from AFM to SL phase observed in RE₂Pt₂Pb,²⁷ unusual magnetization plateaus phenomena under field found in REB₄ series.³⁰ On other side, insulating RE-based oxides are also interesting to unveil the intrinsic SSL physics fully dictated by topological lattice frustrations of RE³⁺

ions, avoiding the influence of exchange interactions mediated by itinerant conduction electrons in metallic systems. But, the related materials are still rare, only $\text{RE}_2\text{BaZnO}_5$ ($\text{RE} = \text{Pr-Ho}$) and its derivatives are magnetically characterized,³¹⁻³³ restrict further explorations of novel magnetism on SSL occupied by RE^{3+} ions. Therefore, discovering new RE-based materials with SSL lattice is highly desirable to uncover the exotic magnetic phenomena, motivating present study.

From the application standpoint, low dimensional RE-based frustrated magnets are attractive as magnetic refrigeration materials in liquid helium temperature regime, enhanced magnetocaloric (MC) effect can be obtained during the adiabatic demagnetization process, because the large magnetic entropy (ΔS_m) arising from highly degenerate magnetic ground states at zero field.³⁴ Additionally, the lower temperature limit for magnetic cooling is determined by magnetic ordering temperature of magnetic reagents. In RE-based frustrated magnets, due to the multiple competing interactions, the suppressed or absence of magnetic ordering will be resultantly endowing them to achieve ultra-low temperatures. Moreover, the variety of spin types, large moments and magnetic anisotropy of RE^{3+} ions make them flexible for designing MC materials working at different field regions. As typical examples, Gd-based frustrated magnets like commercial gadolinium gallium garnet $\text{Gd}_3\text{Ga}_5\text{O}_{12}$ (GGG) as Heisenberg-type antiferromagnets, can bear large MC effect at high fields ($\mu_0 H > 5\text{T}$).³⁵ As comparisons, Ising-anisotropic $\text{Dy}_3\text{Ga}_5\text{O}_{12}$ exhibits better MC performance at low field regions ($\mu_0 H < 2\text{T}$).³⁶

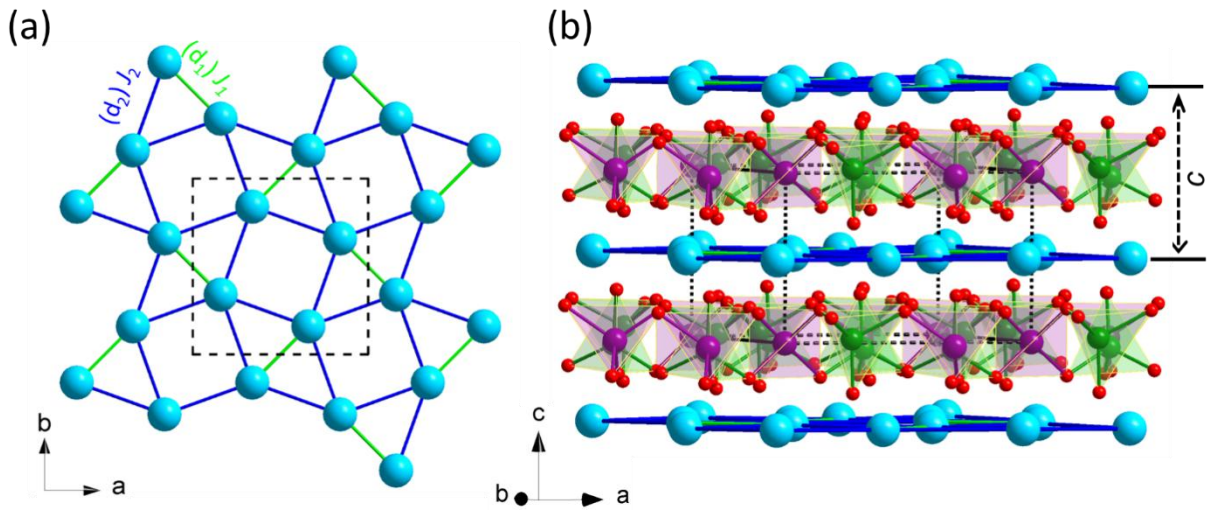


Figure 1. (a) The schematic view of Shastry-Sutherland lattice (SSL), the green and blue lines represent triangle and square bonds. (b) The stacking fashion of SSL layers incorporating of RE^{3+} moments along c axis in $\text{RE}_2\text{Be}_2\text{GeO}_7$, the RE^{3+} layers are well separated by nonmagnetic $[\text{GeBe}_2\text{O}_7]^{6-}$ polyhedrons.

In this work, we report the magnetic properties of $\text{RE}_2\text{Be}_2\text{GeO}_7$ (RE = Pr, Nd, Gd-Yb) melilites comprising the frustrated SSL of RE^{3+} moments. All $\text{RE}_2\text{Be}_2\text{GeO}_7$ compounds crystallize in tetragonal structure with $P\bar{4}2_1m$ space group, which were previously synthesized and structurally characterized firstly by Ochi *et al* and later by Mill *et al* from a structural point of view,^{37,38} but topological lattice geometry on spin frustration has not been studied until now. Our structural analysis reveals that the RE^{3+} ions form the SSL in the *ab* plane and magnetic SSL layers are stacked in an AAA-type fashion well separated by nonmagnetic $[\text{GeBe}_2\text{O}_7]^{4-}$ sheets along *c*-axis. Magnetic characterizations show most $\text{RE}_2\text{Be}_2\text{GeO}_7$ (RE = Pr, Nd, Gd-Yb) compounds except of RE = Tb show no magnetic order down to 2 K despite their dominant antiferromagnetic interactions, where Tb-analogue exhibits AFM transition with Néel temperature $T_N \sim 2.5$ K. The calculated magnetic entropy change ΔS_m reveal that $\text{Gd}_2\text{Be}_2\text{GeO}_7$ has the largest MCE at high fields ($5\text{T} \leq H \leq 7$ T) and $\text{Dy}_2\text{Be}_2\text{GeO}_7$ exhibits better MCE performance at low fields ($H \leq 2$ T), as suitable materials for magnetic refrigeration in liquid helium temperatures.

■ EXPERIMENTAL SECTION

The series of $\text{RE}_2\text{Be}_2\text{GeO}_7$ (RE = Pr, Nd, Gd-Yb) polycrystals were synthesized by a solid state reaction method using GeO_2 (99.99%), BeO (99.5%) and RE oxides RE_2O_3 (RE=Pr, Nd, Gd-Yb; 99.99%) as starting materials. Before using, raw materials RE_2O_3 (RE=Pr, Nd) were pre-dried for 12 hours at 800°C in argon atmosphere. Stoichiometric amounts of the starting materials with mole ratio of RE:Be:Ge=2:2:1 were weighted, ground in glove box. After that, the mixtures were pre-reacted in air at temperature 1100°C for 24 hours. For $\text{RE}_2\text{Be}_2\text{GeO}_7$ (RE=Pr,Nd) samples, the products were re-ground and reacted at temperature of 1200°C-1250°C for 4 days with intermediate grindings. For RE=Gd-Yb compounds, higher reaction temperature of 1300°C is required to obtain pure phase sample.

The phase purity and crystal structure of $\text{RE}_2\text{Be}_2\text{GeO}_7$ were checked by room temperature powder X-ray diffraction (XRD, Rigaku Smartlab) with Cu $K\alpha$ radiation ($\lambda = 1.5418$ Å). The Rietveld refinements of XRD data were performed for structural analysis using Material Studio software.³⁹ The magnetic properties were measured using a commercial SQUID magnetometer (MPMS, Quantum Design) and commercial Physical Property Measurement System (PPMS, Quantum Design) equipped with a vibrating sample magnetometer (VSM) option.

■ RESULTS AND DISCUSSION

Structure descriptions.

All serial $\text{RE}_2\text{Be}_2\text{GeO}_7$ (RE = Pr-Yb) melilites are isostructural and crystallize into tetragonal structure in space group $P\bar{4}2_1m$ (No. 113). In the unit cell, there are six crystallographic sites including one unique RE (Wyckoff site 4e), one Ge (Wyckoff site 2a), one Be (Wyckoff site 4e) and

three types of O (Wyckoff site 2c,2a,8f) sites. Using the crystal structure of $\text{Y}_2\text{Be}_2\text{SiO}_7$ as a starting model,⁴⁰ the experimental and refined XRD patterns for selected $\text{RE}_2\text{Be}_2\text{GeO}_7$ (RE = Pr, Yb) compounds are shown in Figure 2a. The fitted profiles match the experimental data well giving reliability factors R_p (2.95-3.91) and R_{wp} (4.01-5.22). The obtained structural lattice parameters and atomic coordinates are summarized in Table S1 (see Supporting Information), the structural parameters are in accordance with previous report.^{37,38} From the refinement, no significant anti-site mixing between magnetic RE^{3+} and nonmagnetic $\text{Be}^{2+}/\text{Ge}^{4+}$ ions are detected, indicative of ordered arrangement of magnetic RE^{3+} and nonmagnetic $\text{Be}^{2+}/\text{Ge}^{4+}$ cations. The free of site mixing can be related to the difference of ionic radii and coordination number between RE^{3+} and $\text{Be}^{2+}/\text{Ge}^{4+}$ cations, and this is critical to investigate the intrinsic magnetic behaviors from the ordered RE^{3+} moments, avoid the influence of structural disorder on magnetic ground state as the situation in YbMgGaO_4 where the site-mixing occupation of Mg and Ga atoms exist.^{20,41}

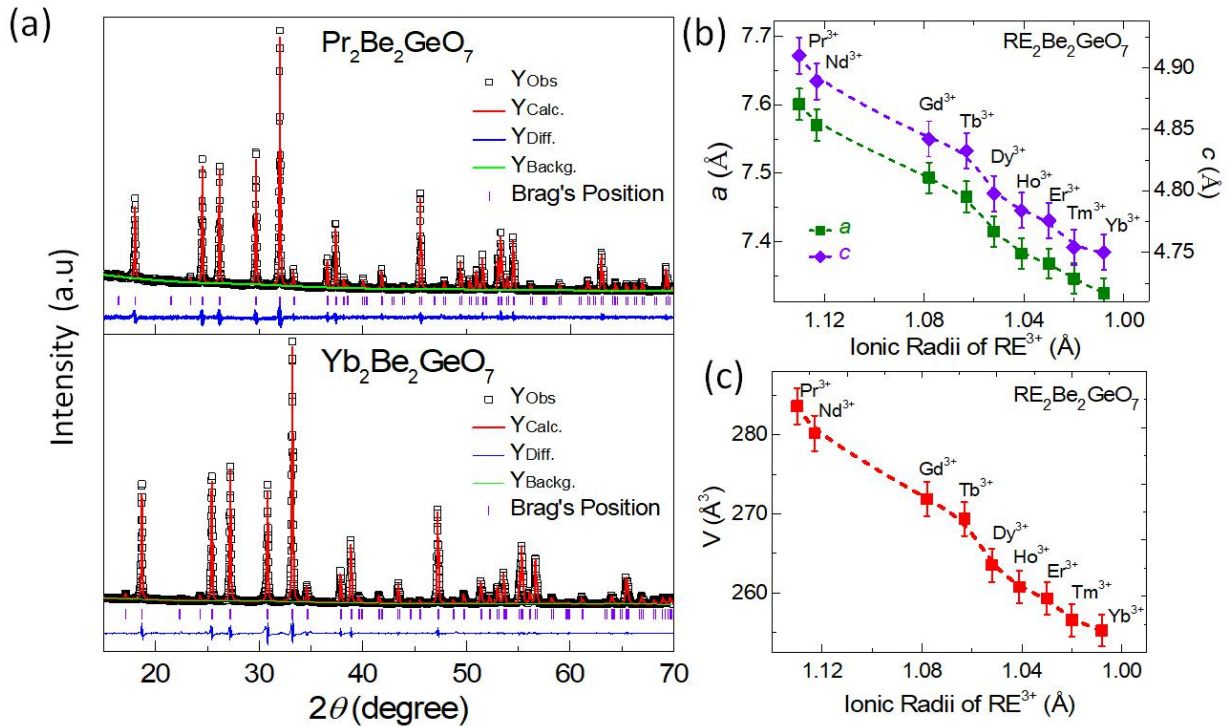


Figure 2. (a) Room-temperature XRD patterns of $\text{RE}_2\text{Be}_2\text{GeO}_7$ (Pr, Gd, Ho, Yb): black squares are experimental data; red lines show calculated patterns, blue line is differences, and violet tick represents Bragg's reflection positions. (b) The variation of lattice parameters and (c) unit-cell volume (V) as a function of ionic radii of RE^{3+} ions in $\text{RE}_2\text{Be}_2\text{GeO}_7$. The dashed lines are given as guides to the eye.

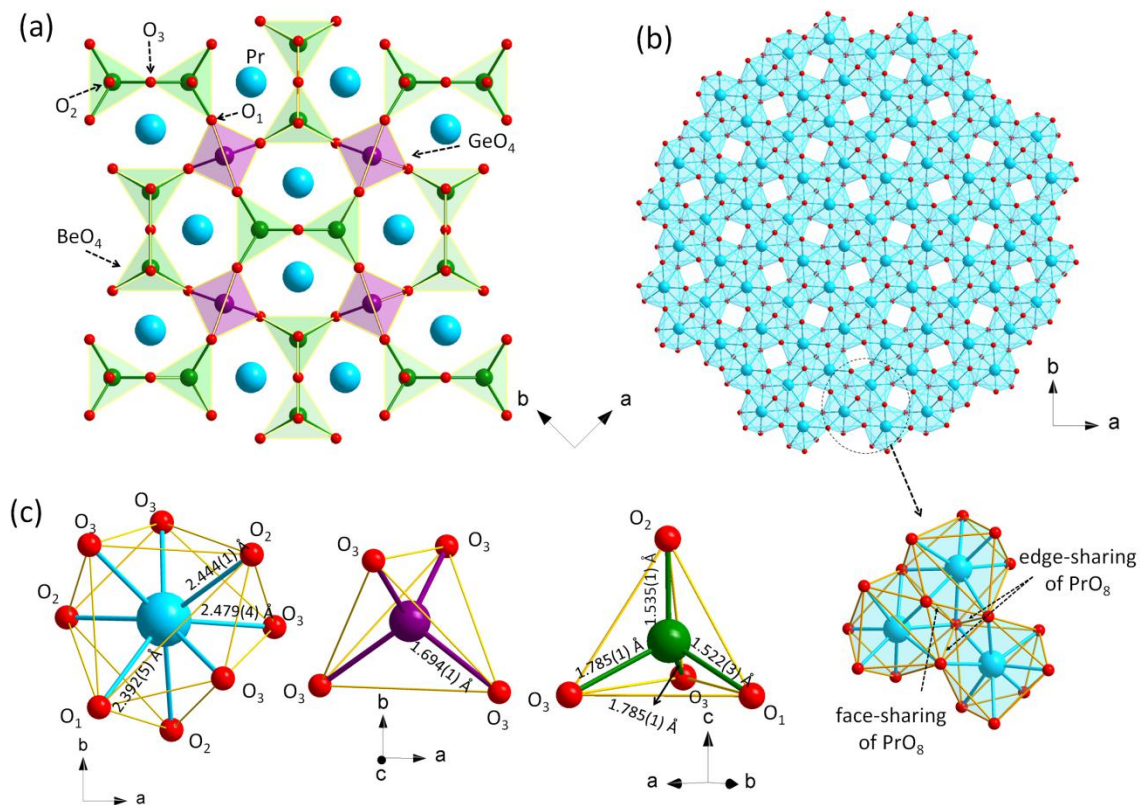


Figure 3. (a) Top view of structural framework of melilite-type $\text{Pr}_2\text{Be}_2\text{GeO}_7$, (b) The connectivity of PrO_8 polyhedrons in the ab plane. (c) The coordination environments of PrO_8 , BeO_4 and GeO_4 polyhedron.

The schematic crystal structure of $\text{Pr}_2\text{Be}_2\text{GeO}_7$ as one representative is presented in Figure 1b, which is also applicable to the other isostructural family members. As seen, magnetic Pr^{3+} ions and nonmagnetic $\text{Be}^{2+}/\text{Ge}^{4+}$ ions are located on separate layers alternatively along the c axis. In the nonmagnetic $[\text{GeBe}_2\text{O}_7]^{6-}$ layers, the corner-sharing GeO_4 tetrahedra and Be_2O_7 distorted tetrahedral dimers build a two-dimensional (2D) network consisted of five-membered rings [see Figure 3a]. The magnetic Pr cations with 8-fold coordination form distorted square Archimedean antiprism residing on neighbouring layers. The detailed coordination environment of oxygen ligands surrounded Pr, Be and Ge cations are shown in Figure 3b, the related interatomic distances and bond angles are provided in Table 1. For distorted BeO_4 tetrahedra, the Be–O distances are 1.522(3) Å, 1.535(1) Å and 1.785(1) Å, and O–Be–O bond angles are 117.0(2)°, 113.9(3)° and 104.5(1)°. The GeO_4 tetrahedra have four Ge–O bond lengths of ~1.694(1) Å and O–Ge–O angles ~109.2(3)°. In the PrO_8 polyhedron, the Pr–O bond distances are ranging from 2.392(3) Å to 2.479(4) Å, and the O–Pr–O angles are 76.1(3)°, 108.2(3)° and 146.1(1)°, respectively. Within the ab plane, the PrO_8 polyhedrons have edge and face-shared connections (see Figure 3c), magnetic Pr^{3+} ions are located on topological Shastry-Sutherland lattice (SSL) pattern. The SSL layers are stacked in an eclipsed

“AAA”-type fashion along *c*-axis, where the inter-plane Pr-Pr distances given by $c=4.910(1)$ Å are larger than the Pr-Pr diagonal bond (~ 3.429 Å) and square bond (~ 4.042 Å). Moreover, considering the well separation of magnetic layers by nonmagnetic Ge/Be-O polyhedrons, an important feature of $\text{Pr}_2\text{Be}_2\text{GeO}_7$ is that its' structure consists of magnetic Pr^{3+} SSL sheets and nonmagnetic $\text{Be}^{2+}/\text{Ge}^{4+}$ layers alternatively along *c* axis.

Table 1. Selected bond distances, bond angles, and interplane and intraplane RE-RE distances of $\text{RE}_2\text{Be}_2\text{GeO}_7$ (RE = Pr, Nd, Gd-Yb) compounds.

RE	Pr	Nd	Gd	Tb	Dy	Ho	Er	Tm	Yb
REO₈									
RE-O ₁ (Å)	2.392(5)	2.352(4)	2.304(1)	2.297(4)	2.267(4)	2.259(1)	2.244(3)	2.236(1)	2.231(5)
RE-O ₂ (Å)	2.444(1)	2.420(2)	2.413(2)	2.405(2)	2.367(3)	2.354(2)	2.302(1)	2.294(3)	2.289(2)
RE-O ₃ (Å)	2.479(4)	2.456(3)	2.413(1)	2.405(3)	2.366(1)	2.359(2)	2.323(4)	2.315(3)	2.310(1)
Intraplane RE-RE (Å)	4.042(3)	4.027(1)	3.988(1)	3.972(1)	3.942(3)	3.927(3)	3.919(1)	3.907(2)	3.896(2)
	3.429(2)	3.409(2)	3.372(1)	3.360(4)	3.339(4)	3.327(4)	3.322(1)	3.312(2)	3.303(5)
Interplane RE-RE (Å)	4.910(1)	4.889(1)	4.842(1)	4.833(4)	4.798(2)	4.784(1)	4.776(2)	4.754(4)	4.750(1)
O ₁ -RE-O ₂ (°)	108.2(1)	109.1(1)	109.5(1)	109.4(2)	109.6(1)	109.6(5)	110.1(5)	110.1(3)	110.0(2)
O ₁ -RE-O ₃ (°)	146.1(1)	146.2(1)	146.4(4)	146.4(2)	146.6(3)	146.7(5)	147.5(4)	147.5(2)	147.5(5)
O ₂ -RE-O ₃ (°)	76.1(1)	75.6(1)	75.2(3)	75.3(1)	75.3(4)	75.3(1)	74.7(2)	74.7(3)	74.8(5)
BeO₄									
Be-O ₁ (Å)	1.522(3)	1.540(1)	1.581(5)	1.575(1)	1.579(1)	1.573(2)	1.524(3)	1.519(4)	1.515(4)
Be-O ₂ (Å)	1.535(1)	1.586(2)	1.564(1)	1.561(1)	1.569(2)	1.565(3)	1.628(2)	1.613(1)	1.609(2)
Be-O ₃ (Å)	1.785(1)	1.742(1)	1.697(3)	1.692(4)	1.656(2)	1.650(2)	1.618(4)	1.621(5)	1.619(1)
O ₁ -Be-O ₂ (°)	117.0(1)	115.1(1)	114.1(5)	114.1(1)	114.8(1)	114.8(1)	117.7(2)	117.7(5)	117.7(2)
O ₁ -Be-O ₃ (°)	104.5(1)	103.8(3)	102.8(3)	102.7(2)	102.4(3)	102.5(4)	104.1(4)	104.2(3)	104.1(2)
O ₂ -Be-O ₃ (°)	113.9(3)	113.9(2)	115.9(3)	115.9(2)	115.9(4)	116.0(4)	114.2(5)	114.1(1)	114.2(4)
GeO₃									
Ge-O ₃ (Å)	1.694(1)	1.707(4)	1.712(4)	1.706(3)	1.716(4)	1.710(4)	1.752(2)	1.746(1)	1.742(1)
O ₃ -Ge-O ₃ (°)	109.2(3)	109.3(2)	109.2(5)	109.1(5)	109.3(5)	109.2(1)	109.1(2)	109.1(2)	109.4(2)

For $\text{RE}_2\text{Be}_2\text{GeO}_7$, both lattice parameters (*a*, *c*) and unit volume *V* decrease almost linearly as decreased RE^{3+} ionic radius, as shown in Figure 2b and 2c. These lattice variations result in the monotonic decrease of RE-RE distances. As seen in Table 1 and Figure S1, the interlayer's spacing (d_{inter}) between SSL layers decreases from $4.910(5)$ Å (RE=Pr) to $4.751(5)$ Å for (RE=Yb), and the nearest and next-nearest RE-RE distance (d_1 and d_2) change from $d_1=3.430(1)$ Å and $d_2=4.041(1)$ Å (RE=Pr) to $d_1=3.301(3)$ Å and $d_2=3.899(1)$ Å for (RE=Yb), respectively. On other side, the value ratio of $d_2/d_1=1.18(1)$ is almost constant irrespective of the variations of RE ions. Considering that the relative strength of intradimer (J_1) and interdimer (J_2) exchanges are sensitive to the RE-RE distances (d_1, d_2) within the SSL plane, which play critical role in determining the magnetic behaviors. Herein, a comparison with another RE-based $\text{RE}_2\text{BaPdO}_5$ was performed, $\text{RE}_2\text{Be}_2\text{GeO}_7$ has

comparable value of d_1 in respect to $d_1=3.0\sim 3.5$ Å of $\text{RE}_2\text{BaPdO}_5$, but have larger d_2/d_1 contrast to $d_2/d_1=1.06\sim 1.07$ of $\text{RE}_2\text{BaPdO}_5$.³² The eclipsed stacking fashion of SSL layers in $\text{RE}_2\text{Be}_2\text{GeO}_7$ is different from $\text{RE}_2\text{BaPdO}_5$ family showing AB-type fashion. Additionally, different local coordinated environments of RE^{3+} ions, resultant crystal-electric field (CEF) effect and $\text{RE}^{3+}\text{-O-RE}^{3+}$ superexchange pathway for above two systems can affect their magnetic behaviors. Therefore, $\text{RE}_2\text{Be}_2\text{GeO}_7$ provides an alternative platform for exploring novel quantum magnetic phases.

Magnetic susceptibilities and isothermal Magnetizations

Temperature (T) dependence of magnetic susceptibilities $\chi(T)$ for $\text{RE}_2\text{Be}_2\text{GeO}_7$ were measured under field cooling condition in an applied field $H=0.1$ T, as shown in Figure 4a-i. Only $\text{Tb}_2\text{Be}_2\text{GeO}_7$ shows antiferromagnetic (AFM) transition characteristics with a peak at $T_N\sim 2.6$ K (see inset of Figure 4d), none of other members exhibit magnetic transitions at $T \geq 2$ K. The Curie-Weiss law $1/\chi(T) = (1/C)(T-\theta_{\text{CW}})$ was used to analyse the inverse susceptibilities $1/\chi(T)$ for extracting the Weiss temperature θ_{CW} and effective moment μ_{eff} , the resultant magnetic parameters are listed in Table 2. The μ_{eff} is calculated by $\mu_{\text{eff}} = (3k_{\text{B}}C/N_{\text{A}})^{1/2}$, where k_{B} is Boltzmann constant and N_{A} is Avogadro's constant. The Curie-Weiss fitting was performed at high temperature (100 K – 300 K) and low temperature ($8 \text{ K} < T < 20 \text{ K}$) regimes, respectively. At high temperatures, $1/\chi(T)$ follows a linear temperature dependence, the fitted value of μ_{eff} is close to theoretical free-ion value $g_{\text{J}}[J(J+1)]^{1/2}$. As decreased temperatures, the slope of $1/\chi(T)$ changes below ~ 80 K and which is especially obvious for $\text{RE}=\text{Pr}$, Nd and Yb compounds, reflects the variation of magnetic interactions and effective moments. This phenomenon is consistent with the magnetic contributions from different $4f$ -manifold excitations due to the crystal electric field (CEF) splitting, where more population of electrons will occupy the CEF ground level as decreased temperatures, leading to the reduced effective moments. For all compounds, negative values of θ_{CW} reveal the dominant AFM type interactions between RE^{3+} moments. Among them, Gd^{3+} is special and has half-filled $4f$ shell ($4f^7$, $S=7/2$, $L=0$) without orbital moments. For $\text{Gd}_2\text{Be}_2\text{GeO}_7$, the negative value of $\theta_{\text{CW}}=-2.4$ K and absence of magnetic transition ($T > 1.8$ K) suggests the dominant AFM exchange interactions between Gd^{3+} moments.

The isothermal magnetization $M(H)$ curves at selected temperatures for $\text{RE}_2\text{Be}_2\text{GeO}_7$ series are shown in Figure 5a-i. Despite $\text{RE}=\text{Pr}$ and Nd , magnetization curves at 2 K of other compounds nearly saturate at 7 T. Among them, $\text{Gd}_2\text{Be}_2\text{GeO}_7$ being a good approximation of Heisenberg antiferromagnet with $S=7/2$ moments, has saturated magnetization $M_{\text{s}}=7.05 \mu_{\text{B}}$ in agreement with the expected value $g_{\text{J}}\mu_{\text{B}} = 7\mu_{\text{B}}$. For $\text{RE}=\text{Dy}$ and Yb , the saturated magnetization is around half of above value with $M_{\text{s}} \sim g_{\text{J}}\mu_{\text{B}}/2$, indicating of easy axis (Ising) anisotropy. For $\text{RE}=\text{Pr}$ and Nd , the observed values of M_{s} at 7 T are quite smaller than expected $M_{\text{s}}=g_{\text{J}}J$ for free $\text{Pr}^{3+}/\text{Nd}^{3+}$ ions. This can be related to their reduced moments at low temperatures due to the low-lying CEF effects.⁴² Further considering the Ising-like magnetic anisotropy, the saturated magnetization of $\text{RE}_2\text{Be}_2\text{GeO}_7$ ($\text{RE}=\text{Pr}$,

Nd) should be $\sim 1.1\text{-}1.3\mu_B/f.u.$, in consistent with the experimental results. In these SSL magnetic oxides, local coordination environment of RE^{3+} ions, resultant different CEF effect and competing dipolar interactions can also affect their magnetic behaviors including the magnetic anisotropic effect, low T effective moment and saturated magnetization. Similar behaviors have been reported for other RE-based magnets such as triangular lattice NaRES_2 ,²² kagome lattice RE_3BWO_9 ⁴³ and one-dimensional $\text{Ca}_4\text{REO}(\text{BO}_3)_3$ systems.⁴⁴

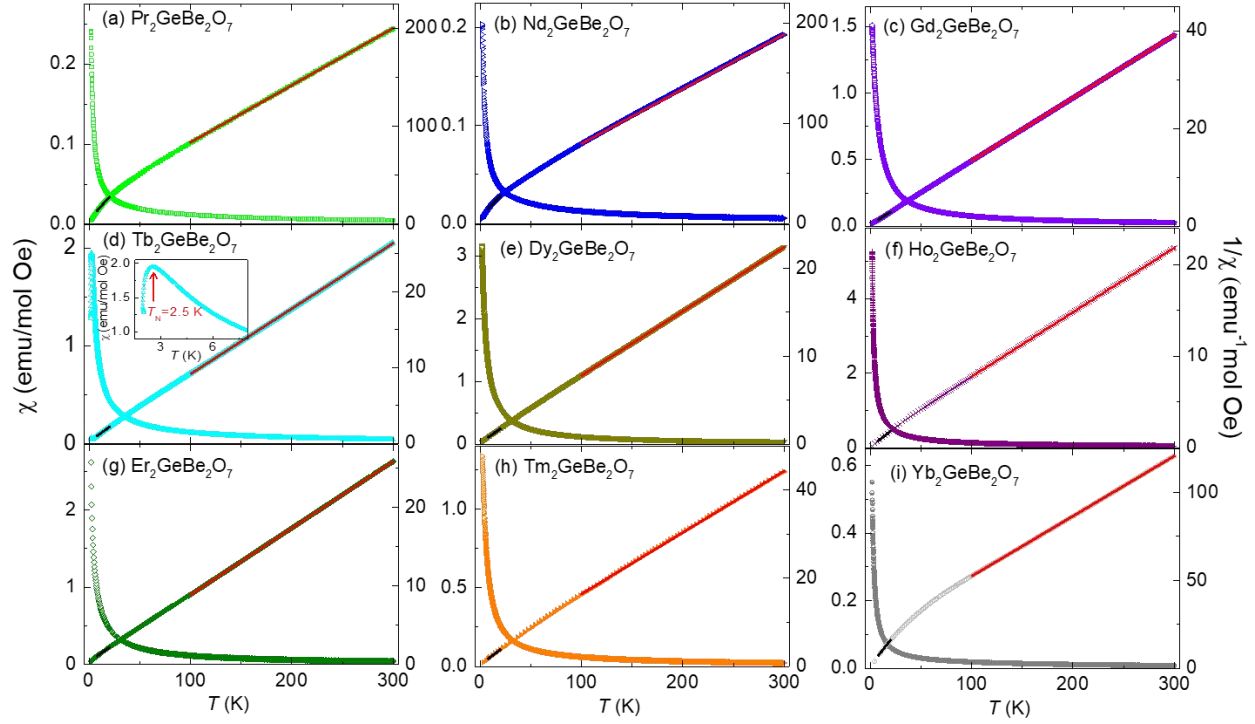


Figure 4. (a-i) Temperature-dependence of susceptibility $\chi(T)$ and inverse susceptibility $1/\chi(T)$ measured at 0.1 T for $\text{RE}_2\text{Be}_2\text{GeO}_7$ (RE = Pr, Nd, Gd-Yb), respectively. The solid red and black lines show the Curie-Weiss fitting at high temperature and low temperature regimes, respectively. The inset in (d) shows the enlarged region of $\chi(T)$ at low temperatures.

For $\text{Tb}_2\text{Be}_2\text{GeO}_7$, $M(H)$ curves at 2 K nearly saturate at ~ 2 T with $M_s = 4.54(5) \mu_B$ slightly smaller than $g_J J \mu_B / 2$ with $J=6$ and $g=3/2$ for free Tb^{3+} ions ($4f^8, ^7F_6$) with $m_J = \pm 6$. Moreover, below T_N , its magnetizations exhibit an inflection point near critical field (H_C) as existence of spin-flop behaviors (see figure 6a). Here, H_C is defined by the peak position of derivative magnetization dM/dH , as shown in the inset of Figure 5d and Figure S3 b. The H_C decreases with increased temperatures towards zero at ~ 2.8 K. Further combing the T_N defined by the peak of magnetic susceptibilities measured at different H (see Figure S3 a), the H - T phase diagram is constructed. The contour plots

using field dependent dM/dH for the phase diagram are shown in figure 6b, the observation of spin-flop transition from AFM to canted-AFM state below T_N reveals the evolution of magnetic configurations. The field induced successive multiple metamagnetic transitions are reported in SSL TbB₄ system,³⁰ as comparisons, further study on field-induced metamagnetic transition based on Tb₂Be₂GeO₇ single crystals are desirable.

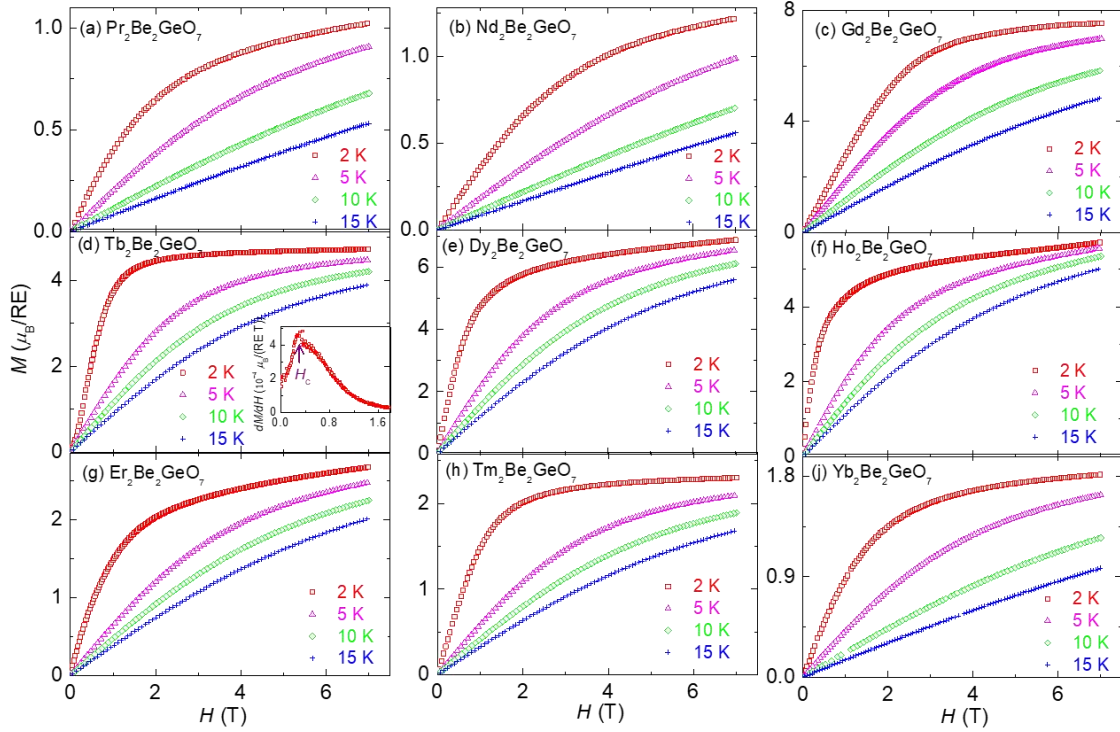


Figure 5. Field-dependence of magnetization $M(H)$ curves at selected temperatures for RE₂Be₂GeO₇ (RE = Pr, Nd, Gd-Yb). The inset in (d) shows the derivative magnetization dM/dH at 2 K.

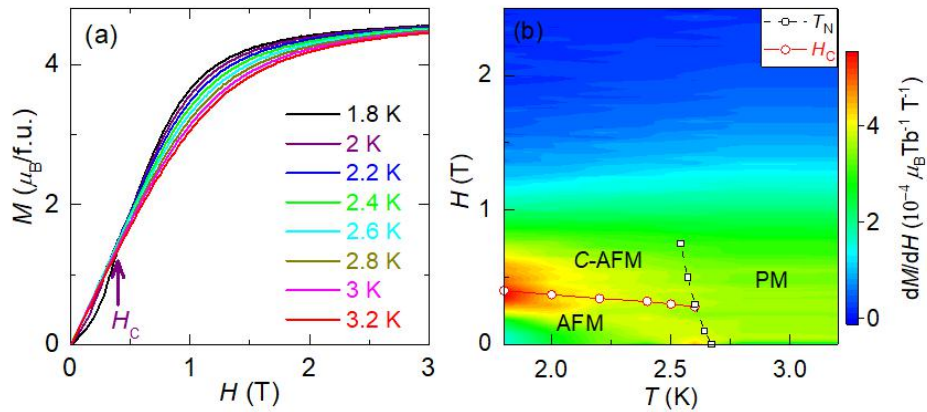


Figure 6. (a) The isothermal $M(H)$ curves for Tb₂Be₂GeO₇ measured at $T \leq 3.2$ K, (b) The constructed field-temperature (H - T) phase diagrams based on dM/dH and $M(T)$ data.

Table 2. Magnetic parameters obtained from the fitting of $\chi(T)$ by the Curie–Weiss law, Curie–Weiss temperatures (θ_{CW}) and effective magnetic moments (μ_{eff}), and the effective moment (μ_{fi}) expected for free ions calculated by $g[J(J+ 1)]^{1/2}$ for for $RE_2Be_2GeO_7$ (RE = Pr, Nd, Gd-Yb).

RE	High T fit (K)	θ_{CW} (K)	μ_{eff} (μ_B)	Low T fit (K)	θ_{CW} (K)	μ_{eff} (μ_B)	μ_{fi} (μ_B)
Pr	100-300	-43.3 (1)	3.70(1)	8-20	-3.61(3)	2.60(1)	3.58
Nd	100-300	-45.6(1)	3.82(1)	8-20	-6.25(5)	2.76(2)	3.62
Gd	100-300	-4.09(5)	7.88(2)	8-20	-2.41(2)	7.79 (1)	7.94
Tb	100-300	-5.95(2)	9.63(1)	8-20	-2.16(2)	9.06(3)	9.72
Dy	100-300	-6.87(6)	10.45(2)	8-20	-1.74(2)	9.92(1)	10.6
Ho	100-300	-10.58(1)	10.66(2)	8-20	-1.05(2)	9.63(1)	10.60
Er	100-300	-4.11	9.70(1)	8-20	-3.45(1)	9.31(2)	9.6
Tm	100-300	-17.5	7.57(1)	8-20	-2.12(1)	6.78(1)	7.6
Yb	100-300	-54.8(1)	4.65(2)	8-20	-0.91	3.18(1)	4.54

Table 3. Dipolar interaction (D) and nearest-neighbour exchange interaction energy (J_{nn}) for $RE_2Be_2GeO_7$ (RE = Pr, Nd, Gd- Yb), where J_{nn} is estimated in the mean-field isotropic approximation.⁴⁵

RE	$D_{intra\text{layer}}$ (K)		$D_{intra\text{layer}}$ (K)	J_{nn} (K) using J	J_{nn} (K) using $J_{eff}=1/2$
	$D_{(\text{square bond})}$	$D_{(\text{square bond})}$			
Pr	0.0639(1)	0.105(1)	0.0358(2)	-0.108(1)	-2.88(2)
Nd	0.0736(2)	0.121(1)	0.0406(1)	-0.152(1)	-5
Gd	0.600(1)	0.981(1)	0.332 (2)	-0.0918(1)	N/A
Tb	0.817(3)	1.35(1)	0.456(3)	-0.0309(1)	-1.73(1)
Dy	1.002(2)	1.66(2)	0.554(2)	-0.0164(1)	-1.39(2)
Ho	0.958(3)	1.56(1)	0.528(1)	-0.0088(1)	-0.84(2)
Er	0.897(2)	1.49(1)	0.497(2)	-0.0325(1)	-2.76(1)
Tm	0.483(2)	0.790(1)	0.267(1)	-0.0303(1)	-1.69(1)
Yb	0.106(2)	0.175(2)	0.059(1)	-0.035(1)	-0.73(1)

The RE^{3+} ions can be divided into two categories, Kramers ions containing odd $4f$ electrons (Nd^{3+} , Dy^{3+} , Er^{3+} and Yb^{3+}) and non-Kramers ions with even numbers of $4f$ electrons (Pr^{3+} , Tb^{3+} , Ho^{3+} and Tm^{3+}). Among them, Gd^{3+} has half-filled $4f$ shell with Heisenberg-like anisotropy, the effective moment is $S_{eff}=7/2$. For other RE-based compounds, effective local spin moment for Kramer's doublet can be described by $S_{eff} = 1/2$ protected by time-reversal symmetry. For non-Kramers ions, the $S_{eff} = 1/2$ ground state can be formed for low crystal-field symmetries, where crystal symmetry

cannot provide enough symmetry operations protecting the degeneracy of the crystal-field levels. Here, due to the absence of inelastic neutron spectroscopy (INS) data of $\text{RE}_2\text{Be}_2\text{GeO}_7$, the CEF and spin anisotropy cannot be accurately determined. Here, the strength of superexchange interactions between local RE^{3+} moments are estimated by the mean-field approximation using $J_{\text{nn}} = 3k_B\theta_{\text{CW}}/zS_{\text{eff}}(S_{\text{eff}}+1)$,⁴⁵ where S_{eff} denominates the total spin number, and z is the number of nearest-neighbor spins (here $z=5$). Considering the strong spin-orbit coupling (SOC) and different spin types of RE^{3+} , both quantum number J and S_{eff} are used to estimate the nearest-neighbor exchange J_{nn} (see Table 3). The dipolar interaction D may be calculated by $D = \mu_0\mu_{\text{eff}}^2/4\pi(r_{\text{nn}})^3$, where r_{nn} is the distance between adjacent RE^{3+} in the SSL layers. Using the low T fitted μ_{eff} , the sizes of dipolar interactions are also listed in Table 3. As seen, the intralayers' dipolar energy is 1.8~2.9 times larger than the interlayers' ones. As an example, for $\text{Yb}_2\text{Be}_2\text{GeO}_7$, the interlayer dipole interaction ($D_{\text{interlayer}} \sim 0.059$ K) is ~ 2.4 times weaker than the average value of intralayers' interaction ($D_{\text{intra-layer}} \sim 0.14$ K). The simultaneous mediation by exchange/dipolar interactions, orbital hybridization and presence of varies spin types (Ising, Heisenberg, and planar XY) in $\text{RE}_2\text{Be}_2\text{GeO}_7$ melilites would be important factors, which should be considered to determine the magnetic interactions and magnetic ground states. Moreover, considering similar geometric networks of RE-O-RE or RE-O-O-RE superexchange pathway in this family, the highest magnetic ordering temperature of $\text{Tb}_2\text{Be}_2\text{GeO}_7$ reveals other factors like orbital hybridization inherent to different 4f orbit on magnetic exchange interactions should be considered. Similar behavior in Quasi-One-Dimensional RE-based magnets $\text{Ca}_4\text{LnO}(\text{BO}_3)_3$ has also been reported,⁴⁴ where only $\text{Ca}_4\text{TbO}(\text{BO}_3)_3$ compound undergo magnetic transition above 2 K ($T_N = 3.6$ K).

Magnetocaloric effect

The RE-based compounds are quite suitable as magnetic refrigeration materials, which can show large magnetocaloric (MC) effect due to the large number of unpaired spins and great magnetic moments. In Figure 5, four members for RE = Gd, Tb, Dy, Ho are identified to have relatively large magnetizations, then we focus on the MC studies on above compounds. Magnetic entropy changes (ΔS_m) were calculated from isothermal process of magnetization by employing Maxwell's relation:⁴⁶ $\Delta S_m = \int_{H_i}^{H_f} \left(\frac{\partial M}{\partial T} \right)_H dH$, where H_i (usually $H_i=0$) and H_f represent the initial and final values of magnetic field, respectively. The obtained field dependence of $-\Delta S_m$ at 2 K are shown in Figure 7. In this family, $\text{Gd}_2\text{Be}_2\text{GeO}_7$ shows the optimal MCE in large field regions ($5 \text{ T} \leq H \leq 7 \text{ T}$) with maximum $-\Delta S_m = 54.8 \text{ J K}^{-1} \text{ kg}^{-1}$ at 2 K, while $\text{Dy}_2\text{Be}_2\text{GeO}_7$ has the best MCE at low fields $H \leq 2 \text{ T}$, where 2 T is the largest field attainable with permanent magnets. This MCE at low field is more attractive for practical applications free of cryogenes.

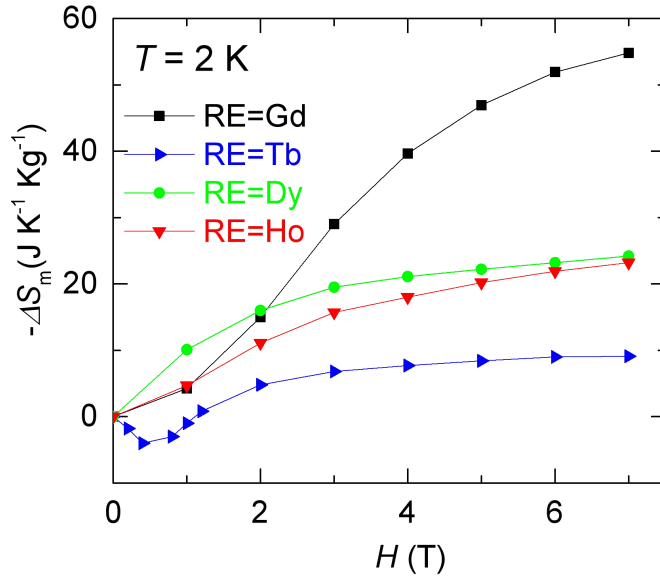


Figure 7. The field dependence of magnetic entropy change ΔS_m for $RE_2Be_2GeO_7$ (RE = Gd,Tb,Dy,Ho) at 2 K.

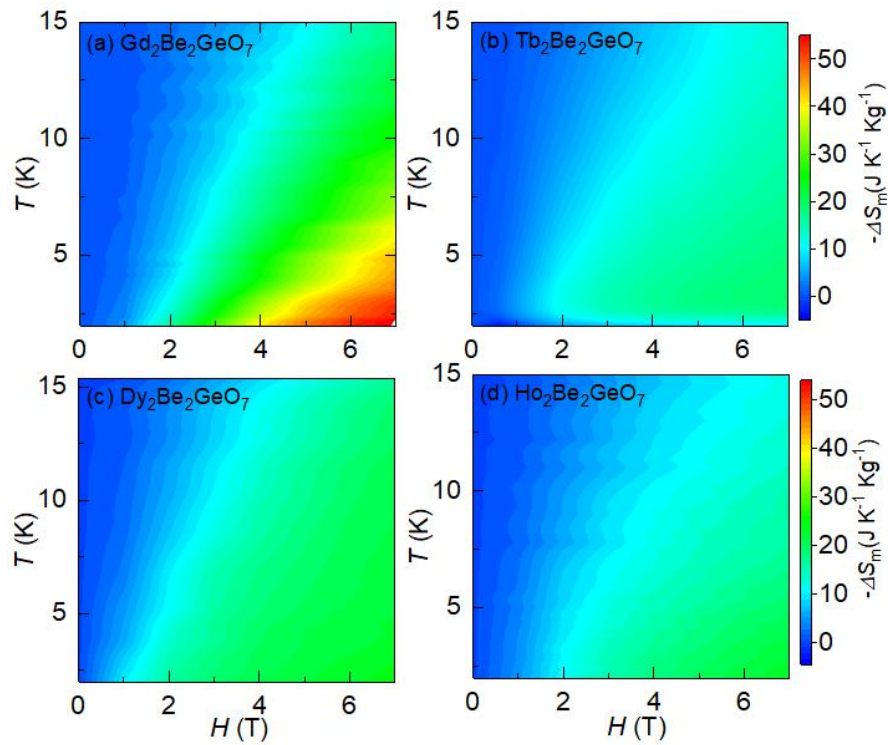


Figure 8. (a-d) The contour plots of obtained $-\Delta S_m$ as function of temperature (2 K- 15 K) and field for $RE_2Be_2GeO_7$ (RE = Gd,Tb,Dy,Ho).

Moreover, the contour plots of obtained $-\Delta S_m$ as function of temperature (2 K- 15 K) and field for $RE_2Be_2GeO_7$ (RE = Gd, Tb, Dy, Ho) melilites are given in Figure. 8. As compared to the benchmark MC material $Gd_3Ga_5O_{12}$ (GGG) or $Dy_3Ga_5O_{12}$ (DGG), the obtained MCE of $RE_2Be_2GeO_7$ (RE=Gd, Dy) is impressive, high field ($\Delta H=7$ T) $\Delta S_m=54.8$ J K⁻¹ Kg⁻¹ of $Gd_2Be_2GeO_7$ is much larger than that of GGG ($-\Delta S_m = 38.5$ J K⁻¹ Kg⁻¹) at 2 K.^{35,36} In lower field change $\Delta H=2$ T, MCE performance of $Dy_2Be_2GeO_7$ (16.1 J K⁻¹ kg⁻¹) also surpasses DGG (11.0 J K⁻¹ kg⁻¹) and GGG (14.6 J K⁻¹ kg⁻¹) at 2 K, see Table S1. Additionally, $Tb_2Be_2GeO_7$ exhibits maximum $-\Delta S_m$ at 2.8 K for all fields, around the ordering temperature $T_N\sim 2.5$ K, then $-\Delta S_m$ fall off on both side temperatures, as observed in $RE_3CrGa_4O_{12}$ (RE = Tb, Dy, Ho).^{36,47} The MCE of $Dy_2Be_2GeO_7$ has remarkable values and weak temperature dependence between 2 and 15 K. The large MCE make $RE_2Be_2GeO_7$ as competitive magnetic refrigeration materials at liquid Helium temperatures, further optimised magnetocaloric efficiency at different temperature and field regimes could be realized by partial chemical substitutions or solid-state solutions such as $Gd_{2-x}Dy_xBe_2GeO_7$.

According to the SSL models, its magnetic ground states strongly depend on the intra- and inter-dimer couplings ratio J_2/J_1 strength, which is experimentally confirmed by the well-studied spin-1/2 dimerized SSL magnets $SrCu_2(BO_3)_2$.¹⁴⁻¹⁷ As comparison, magnetic ground states of RE-based SSL magnets should also be affected by the anisotropic spin exchange interactions due to the strong spin-orbital-entanglement and CEF effects. As an example, the present $Yb_2Be_2GeO_7$ will provide comparative study on magnetic ground state between Cu^{2+} ($S=1/2$) and Yb^{3+} ($J_{eff}=1/2$) SSL based systems. The varies of different spin types (Ising, Heisenberg, and planar XY) in $RE_2Be_2GeO_7$ melilites would be attractive for discovering diverse novel magnetic ground states, such as spin liquid state, dimers state, etc. New theoretical model combing the above effects and extensive ultra-low-temperature experimental studies based on high quality single crystals will be significant to elucidating the ground state of these systems, and the availability of $RE_2Be_2GeO_7$ single crystals will be highly desirable to unveil anisotropic magnetocaloric effect.

■ CONCLUSIONS

A new family of RE-based magnets $RE_2Be_2GeO_7$ (RE = Pr, Nd, Gd-Yb) were synthesized, where RE^{3+} ions are located on the SSL within the *ab* plane. Structurally, the SSL layers exhibit the eclipsed AAA-type stacking in comparison with the AB-type fashion of RE_2BaZnO_5 . In this family, most $RE_2Be_2GeO_7$ (RE = Pr, Nd, Gd-Yb) compounds except of RE = Tb show no magnetic order down to 2 K, where $Tb_2Be_2GeO_7$ exhibits AFM transition with Néel temperature $T_N\sim 2.5$ K and field-induced spin flop behaviors ($T < T_N$). The calculated magnetic entropy change ΔS_m reveal large magnetocaloric effect (MCE) for $RE_2Be_2GeO_7$ (RE =Gd, Dy) in liquid helium temperature regimes, $Gd_2Be_2GeO_7$ shows the optimal MCE (54.8 J K⁻¹ Kg⁻¹) at 7 T and $Dy_2Be_2GeO_7$ has the maximum

MCE ($16.1 \text{ J K}^{-1} \text{ kg}^{-1}$) at 2 T as suitable materials for magnetic refrigeration. Moreover, the present SSL magnets incorporating strong spin orbit coupled 4f ions with $J_{\text{eff}}=1/2$ spin enable the possibility to explore novel quantum magnetic phases beyond the $\text{SrCu}_2(\text{BO}_3)_2$ as typical $S=1/2$ Cu^{2+} -based SSL magnet.

■ ASSOCIATED CONTENTS

Supporting information.

The room-temperature XRD spectra and refined lattice parameters of $\text{RE}_2\text{Be}_2\text{GeO}_7$, magnetic results of $\text{Tb}_2\text{Be}_2\text{GeO}_7$ are provided.

■ AUTHOR INFORMATION

Corresponding Author

Zhaoming Tian –*Wuhan National High Magnetic Field Center and School of Physics, Huazhong University of Science and Technology, Wuhan, 430074, P. R. China;*
orcid.org/0000-0001-6538-3311; Email:tianzhaoming@hust.edu.cn

Authors

Malik Ashtar –Wuhan National High Magnetic Field Center and School of Physics, Huazhong University of Science and Technology, Wuhan, 430074, P. R. China

Yuming Bai –Wuhan National High Magnetic Field Center and School of Physics, Huazhong University of Science and Technology, Wuhan, 430074, P. R. China

Longmeng Xu –Wuhan National High Magnetic Field Center and School of Physics, Huazhong University of Science and Technology, Wuhan, 430074, P. R. China

Zongtang Wan –Wuhan National High Magnetic Field Center and School of Physics, Huazhong University of Science and Technology, Wuhan, 430074, P. R. China

Zijun Wei –Wuhan National High Magnetic Field Center and School of Physics, Huazhong University of Science and Technology, Wuhan, 430074, P. R. China

Yong Liu –School of Physics, Wuhan University, Wuhan 430072, Peoples R China.

Mohsin Ali Marwat –College of Materials Science and Engineering, Huazhong University of Science and Technology, Wuhan 430074, PR China

Notes

The authors declare no competing financial interest.

■ ACKNOWLEDGEMENTS

We acknowledge financial support from the National Natural Science Foundation of China (Grant No. 11874158 and 11604281), and Fundamental Research Funds for the Central Universities (Grant No. 2018KFYYXJJ038 and 2019KFYXKJC008). We would like to thank the staff of the analysis centre of Huazhong University of Science and Technology for their assistance in structural characterization and analysis.

■ REFERENCES

- (1) Moessner, R.; and Ramirez, A. P. Geometrical frustration. *Phys. Today*. **2006**, 59, 24.
- (2) Balents, L. Spin liquids in frustrated magnets. *Nature* **2010**, 464, 199-208.
- (3) Shimizu, Y.; Miyagawa, K.; Kanoda, K.; Maesato, M.; Saito, G. Spin-liquid state in an organic mott insulator with a triangular lattice. *Phys. Rev. Lett.* **2003**, 91, 107001
- (4) Kitagawa, K.; Takayama, T.; Matsumoto, Y.; Kato, A.; Takano, R.; Kishimoto, Y.; Bette, S.; Dinnebier, R.; Jackeli, G.; Takagi, H. A spin-orbital-entangled quantum liquid on a honeycomb lattice. *Nature* **2018**, 554,7692.
- (5) Mukherjee, P.; Hamilton, A. C. S.; Glass, H. F. J.; Dutton S. E. Sensitivity of magnetic properties to chemical pressure in lanthanide garnets $\text{Ln}_3\text{A}_2\text{X}_3\text{O}_{12}$, Ln= Gd, Tb, Dy, Ho, A= Ga, Sc, In, Te, X= Ga, Al, Li. *J. Phys.: Condens. Matter*. **2017**, 29, 405808.
- (6) Lawler, M. J.; Kee, H. Y.; Kim, Y. B.; and Vishwanath, A. Topological Spin Liquid on the Hyperkagome Lattice of $\text{Na}_4\text{Ir}_3\text{O}_8$. *Phys. Rev. Lett.* **2008**, 100, 227201.
- (7) Wen, J.; Yu, S.L. Li, S.; Yu, W.; Li, J. X. Experimental identification of quantum spin liquids. *NPJ. Quantum Mater.* **2019**, 4, 12.
- (8) Yamashita, S.; Nakazawa, Y.; Oguni, M.; Oshima, Y.; Nojiri, H.; Shimizu, Y.; Miyagawa, K.; and Kanoda, K. Thermodynamic properties of a spin-1/2 spin-liquid state in a k-type organic salt. *Nat. Phys.* **2008**, 4, 459-462.
- (9) Han, T.-H.; Helton, J. S.; Chu, S.; Nocera, D.G.; Rodriguez-Rivera, J.A.; Broholm, C.; Lee, Y.S. Fractionalized excitations in the spin-liquid state of a Kagome-lattice antiferromagnet. *Nature* **2012**, 492, 406-410.
- (10) Khuntia, P.; Velazquez, M.; Barthélemy, Q.; Bert, F.; Kermarrec, E.; Legros, A.; Bernu, B.; Messio, L. Zorko A.; Mendels P. Gapless ground state in the archetypal quantum kagome antiferromagnet $\text{ZnCu}_3(\text{OH})_6\text{Cl}_2$. *Nat. Phys.* **2020**, 16, 469–474.
- (11) Feng, Z.L.; Li, Z.; Meng, X.; Yi, W.; Wei, Y.; Zhang, J.; Wang, Y.C.; Jiang, W; Liu, Z.; Li, S. Y.; Liu, F.; Luo J.L.; Li, S.L.; Zheng, G.Q.; Meng, Z.Y.; Mei, J.W.; Shi, Y.G. Gapped spin-1/2 spinon

excitations in a new Kagome quantum spin liquid compound $\text{Cu}_3\text{Zn}(\text{OH})_6\text{FBr}$. *Chin. Phys. Lett.* **2017**, 34, 077502.

(12) Sutherland, B.; Shastry, B. S. Exact ground state of a quantum mechanical antiferromagnet. *Physica*, **1981**, 1088, 1069.

(13) Miyahara, S.; Ueda, K. Exact dimer ground state of the two dimensional Heisenberg spin system $\text{SrCu}_2(\text{BO}_3)_2$. *Phys. Rev. Lett.* **1999**, 82, 3701-3704.

(14) Kageyama, H.; Yoshimura, K.; Stern, R.; Mushnikov, N. V.; Onizuka, K.; Kato, M.; Kosuge, K.; Slichter, C. P.; Goto, T.; Ueda, Y. Exact dimer ground state and quantized magnetization plateaus in the two-dimensional spin system $\text{SrCu}_2(\text{BO}_3)_2$. *Phys. Rev. Lett.* **1999**, 82, 3168.

(15) Kodama, K.; Takigawa, M.; Horvatic, M.; Berthier, C.; Kageyama, H.; Ueda, Y.; Miyahara, S.; Becca, F.; Mila, F. Magnetic superstructure in the two-dimensional quantum antiferromagnet $\text{SrCu}_2(\text{BO}_3)_2$. *Science*, **2002**, 298, 395.

(16) Onizuka, K.; Kageyama, H.; Narumi, Y.; Kindo, K.; Ueda, Y.; Goto, T. 1/3 magnetization plateau in $\text{SrCu}_2(\text{BO}_3)_2$ - stripe order of excited triplets. *J. Phys. Soc. Jpn.* **2000**, 69, 1016.

(17) Guo, J.; Sun, G. Y.; Zhao, B. W.; Wang, L.; Hong, W. S.; Sidorov, V. A.; Ma, N.; Wu, Q.; Li, S. L.; Meng, Z. Y.; Sandvik, A. W.; Sun, L.L. Quantum phases of $\text{SrCu}_2(\text{BO}_3)_2$ from high-pressure thermodynamics. *Phys. Rev. Lett.* **2020**, 124, 206602.

(18) Rau, J. G.; Gingras, M. J. P. Frustrated quantum rare-earth pyrochlores. *Annual Rev. Condens. Matter. Phys.* **2019**, 10, 357.

(19) Sanders, M. B.; Krizan, J. W.; Cava, R. J. $\text{RE}_3\text{Sb}_3\text{Zn}_2\text{O}_{14}$ (RE = La, Pr, Nd, Sm, Eu, Gd): a new family of pyrochlore derivatives with rare earth ions on a 2D Kagomé lattice. *J. Mater. Chem. C*, **2016**, 4, 541.

(20) Li, Y. S.; Liao, H. J.; Zhang, Z.; Li, S. Y.; Jin, F.; Ling, L. S.; Zhang, L.; Zou, Y. M.; Pi, L.; Yang, Z. R.; Wang, J. F.; Wu, Z. H.; Zhang, Q. M. Gapless quantum spin liquid ground state in the two-dimensional spin-1/2 triangular antiferromagnet YbMgGaO_4 . *Scientific Reports*, **2015**, 5, 6419.

(21) Ashtar, M.; Marwat, M. A.; Gao, Y. X.; Zhang, Z. T.; Pi, L.; Yuan, S. L.; Tian, Z. M. $\text{REZnAl}_{11}\text{O}_{19}$ (RE=Pr, Nd, Sm-Tb): a new family of ideal 2D triangular lattice frustrated magnets. *J. Mater. Chem. C*. **2019**, 7, 10073.

(22) Liu, W.; Zhang, Z.; Ji, J.; Liu, Y.; Li, J.; Wang, X.; Lei, H.; Chen, G.; Zhang, Q. Rare-earth chalcogenides: A large family of triangular lattice spin liquid candidates. *Chin. Phys. Lett.* **2018**, 35, 117501.

(23) Bramwell, S. T.; Harris, M. J. The history of spin ice, *J. Phys. Condens. Matter*. **2020**, 32, 374010.

(24) Gao, B.; Chen, T.; Tam, D. W.; Huang, C. L.; Sasmal, K.; Adroja, D. T.; Ye, F.; Cao, H. B.; Sala, G.; Stone, M. B.; Baines, C.; Verezhak, J. A. T.; Hu, H. Y.; Chung, J. H.; Xu, X. H.; Cheong, S. W.; Nallaiyan, M.; Spagna, S.; Maple, M. B.; Nevidomskyy, A. H.; Morosan, E. Chen, G.; Dai, P.C.

Experimental signatures of a three-dimensional quantum spin liquid in effective spin-1/2 $\text{Ce}_2\text{Zr}_2\text{O}_7$. *Nat. Phys.* **2019**, 15, 1052.

(25) Shen, Y.; Liu, C. L.; Qin, Y. Y.; Shen, S. D.; Li, Y. D.; Bewley, R.; Schneidewind, A.; Chen, G.; Zhao, J. Intertwined dipolar and multipolar order in the triangular-lattice magnet TmMgGaO_4 . *Nat. Comm.* **2019**, 10, 4530.

(26) De Farias, C. S.; De Carvalho, V. S.; Miranda, E.; Pereira, R. G. Quadrupolar spin liquid, octupolar kondo coupling, and odd-frequency superconductivity in an exactly solvable model. *Phys. Rev B* **2020**, 102, 075110.

(27) Kim, M. S.; Bennett, M. C.; Aronson, M. C. $\text{Yb}_2\text{Pt}_2\text{Pb}$: Magnetic frustration in the Shastry-Sutherland lattice. *Phys. Rev. B*, **2008**, 77, 144425.

(28) Kabeya, N.; Takahara, S.; Satoh, N.; Nakamura, S.; Katoh, K.; Ochiai A. Antiferromagnetic ground state and heavy-fermion behavior in $\text{Ce}_2\text{Pt}_2\text{Pb}$. *Phys. Rev. B* **2018**, 98, 035131.

(29) Etourneau, J.; Mercurio, J. P.; Berrada, A.; Hagenmuller, P.; Georges, R.; Bourezg, R.; Gianduzzo, J. C. The magnetic and electrical properties of some rare earth tetraborides. *J. Less-Com. Metal.* **1979**, 67, 531-539

(30) Yoshii, S.; Yamamoto, T.; Hagiwara, M.; Michimura, S.; Shigekawa, A.; Iga, F.; Takabatake, T.; Kindo, K. Multistep magnetization plateaus in the Shastry-Sutherland system TbB_4 . *Phys. Rev. Lett.* **2008**, 101, 087202.

(31) Goya, G. F.; Mercader, R. C.; Causa, M. T.; Tovar, M.; Magnetic properties of $\text{P nma-R}_2\text{BaZnO}_5$ oxides (R = Sm, Eu, Dy and Ho). *J. Phys.: Condens. Matter.* **1996**, 8, 8607–8612.

(32) Ozawa, T. C.; Taniguchi, T.; Kawaji, Y.; Mizusaki, S.; Nagata, Y.; Noro, Y.; Samata, H.; Mitamura, H.; Takayanagif, S. Magnetization and specific heat measurement of the Shastry–Sutherland lattice compounds: $\text{Ln}_2\text{BaPdO}_5$ (Ln = La, Pr, Nd, Sm, Eu, Gd, Dy, Ho). *J. Alloy. Comp.* **2008**, 448 96–103.

(33) Ishii, Y.; Chen, J.; Yoshida, H. K.; Oda, M.; Christianson, A. D.; Yamaura, K. High-pressure synthesis, crystal structure, and magnetic properties of the Shastry-Sutherland-lattice oxides $\text{BaLn}_2\text{ZnO}_5$ (Ln = Pr, Sm, Eu). *J. Solid State Chem.* **2020**, 289, 121489.

(34) Zhitomirsky, M. E. Enhanced magnetocaloric effect in frustrated magnets. *Phys. Rev B* **2003**, 67, 104421.

(35) Hamilton, A.C. S.; Lampronti, G.I.; Rowley, S.E.; Dutton, S.E. Enhancement of the magnetocaloric effect driven by changes in the crystal structure of Al-doped GGG, $\text{Gd}_3\text{Ga}_{5-x}\text{Al}_x\text{O}_{12}$ ($0 \leq x \leq 5$). *J. Phys. Condens. Matter.* **2014**, 26, 116001.

(36) Mukherjee, P.; Dutton, S. E. Enhanced magnetocaloric effect from Cr substitution in Ising Lanthanide Gallium Garnets $\text{Ln}_3\text{CrGa}_4\text{O}_{12}$ (Ln=Tb, Dy, Ho). *Adv. Funct. Mater.* **2017**, 27,1701950.

- (37) Ochi, Y.; Morikawa, H.; Minato, I.; Marumo, F. Preparation and magnetic property of new rare earth compounds $R_2GeBe_2O_7$ ($R=La, Pr, Sm, Gd, Dy, Er$) and $Y_2GeBe_2O_7$. *Mat. Res. Bull.* **1982**, 17, 911-916.
- (38) Mill B. V.; Baibakova, G. D. New compounds with Melilite structure: $Ln_2SiBe_2O_7$ ($Ln=Nd-Eu, Tb, Ho-Lu$) and $Ln_2GeBe_2O_7$ ($Ln=Nd, Eu, Tb, Ho, Tm-Lu$). *Russ. J. Inorg. Chem.* **1990**, 35, 341-343.
- (39) Rietveld H. M. *J. Appl. Crystallogr.* **1969**, 2, 65.
- (40) Bartram, S. F. Crystal Structure of $Y_2SiBe_2O_7$. *Acta Crystallogr.* **1969**, B25, 791.
- (41) Ma, Z.; Wang, J. H.; Dong, Z. Y.; Zhang, J.; Li, S. C.; Zheng, S. H.; Yu, Y. J.; Wang, W.; Che, L. Q.; Ran, K. J.; Bao, S.; Cai, Z. W.; Cermak, P.; Schneidewind, A.; Yano, S.; Gardner, J. S.; Lu, X.; Yu, S.L.; Liu, J. M.; Li, S. Y.; Li, J. X.; Wen, J. S. Spin-glass ground state in a triangular-lattice compound $YbZnGaO_4$. *Phys. Rev. Lett.* **2018**, 120, 087201.
- (42) Scheie, A.; Dasgupta, S.; Sanders, M.; Sakai, A.; Matsumoto, Y.; Prisk, T. R.; Nakatsuji, S.; Cava, R. J.; Broholm, C. Homogeneous reduced moment in a gapful scalar chiral kagome antiferromagnet. *Phys. Rev B* **2019**, 100, 024414.
- (43) Ashtar, M.; Guo, J.; Wan, Z.; Wang, Y.; Gong, G.; Liu, Y.; Su, Y.; Tian, Z. A new family of disorder-free Rare-Earth-based kagomé lattice magnets: structure and magnetic characterizations of RE_3BWO_9 ($RE=Pr, Nd, Gd-Ho$) Boratungstates. *Inorg. Chem.* **2020**, 59, 5368-5376.
- (44) Kelly, N. D.; Dutton, S. E. Magnetic properties of Quasi-one-dimensional Lanthanide calcium oxyborates $Ca_4LnO(BO_3)_3$. *Inorg. Chem.* **2020**, 59, 9188-9155.
- (45) Greedan, J. E. Geometrically frustrated magnetic materials. *J. Mater. Chem.* **2001**, 11, 37-53.
- (46) Pecharsky, V. K. Gschneidner, K.A. Magnetocaloric effect and magnetic refrigeration. *J. Mag. Magn. Mater.* **1999**, 200, 44-56.
- (47) Muniraju, N. K. C.; Baral, R.; Tian, Y.; Li, R.; Poudel, N. Gofryk, K.; Barisic, N.; Kiefer, B.; Ross, Jr, J. H.; Nair, H. S. Magnetocaloric Effect in a Frustrated Gd-Garnet with No Long-Range Magnetic Order. *Inorg. Chem.* **2020**, 59, 15144-15153.